International Journal of Refractory Metals and Hard Materials 110 (2023) 106033

Contents lists available at ScienceDirect

International Journal of Refractory Metals and Hard Materials

journal homepage: www.elsevier.com/locate/IJRMHM

Oxidation behaviour and its effect on fracture toughness of Niobium metal

Karthikeyan Ramachandran *, Yasith C. Jayakody, Doni Daniel Jayaseelan *

Department of Aerospace and Aircraft Engineering, Kingston University, Roehampton Vale Campus, London SW15 3DW, UK

ARTICLE INFO

Keywords:
Niobium
Oxidation behaviour
Oxidation kinetics
Indentation fracture toughness and scanning electron microscopy

ABSTRACT

Niobium metal was studied for its oxidation behaviour at different temperatures (800, 1000 & 1200 °C) and time (1, 3 & 5 h). The study revealed that Nb underwent oxidation forming pro-active Nb oxides with initial formation of meta-stable $Nb_{12}O_{29}$ which forms as an oxidisation resistant layer. However, formation of Nb_2O_5 from a meta-sable $Nb_{12}O_{29}$ did not act as protective layer as it exposed underneath to further oxidation leading to cracks. The oxidation kinetics of Nb shown a linear behaviour and the devised mathematical model using Deal Grove determined the thickness of oxide layers. The un-protectiveness of Nb_2O_5 was verified by the Vickers hardness (8.06 ± 0.4 GPa) and indentation fracture toughness (28.14 ± 0.4 MPa.$m^{1/2}$) of material which decreased with increase in oxidation temperature.

1. Introduction

Niobium (Nb) and its alloys play a significant role in modern material technology owing to its abilities in harsh environments. The behaviour and properties of Nb and its alloys make the metal unique for its essential applications for aerospace, electronics and defence sectors [1]. However, owing to elevated temperatures heat transfer and thermal controlling of aerospace components could affect the metals and alloys hence leading to the requirement of barrier coatings which give protection to the components from various environmental conditions [2,3]. Niobium is one of the metals which can potentially replace aluminium and its alloys in aerospace applications and as an additive to other high temperature metallic components in hot section of components owing to its higher hardness, and higher thermal stabilities [4,5]. This makes Nb suitable for elevated temperature and structural applications with a potential to replace various internal aerospace structures and other applications. However, material utilised for high-temperature applications should possess good oxidation resistance and retaining its mechanical properties at high temperatures [6,7].

Gulbransen et al. studied Nb metal at different temperatures and determined that it obeys the parabolic law of oxidation between 200 °C to 375 °C with oxide layer formation at 200 °C acting to prevent further oxidation unless the temperature is increased. On the other hand, under water vapour environments a linear rate was viewed until 1200 °C with irregular behaviours at 400 °C for the moisture environment [8]. Few studies reported that oxidation properties of Nb are poor even though the metal is one of the lightest refractory metals with a high melting point [5]. Tuffias et al. supported the poor oxidation behaviour by reporting oxidation layers formation on the surfaces of Nb were non-protective with a tendency to crack which could lead to the expose the surfaces of metal [9].

Though there have been extensive studies on Nb based structural alloys which focused on reducing the oxidation kinetics by modifying oxidation products, most of these studies were unsuccessful in determining the formation of oxide layers other than Nb_2O_5 which was considered non-protective oxide [10,11]. Most of the previously reported oxidation studies were based on alloys and analyses related to pure Nb is limited. Further, most of the studies cited above show anomalies on the oxidation behaviours even with Nb as an alloy. Hence, this research intends to fill the gap in atmospheric oxidation behaviour of pure Nb metal at different temperatures and time along with its mechanical properties were also evaluated.

2. Experimental details

Commercially available Niobium metal plates of dimension 150 mm × 150 mm × 3 mm were obtained from Edgetech Industries LLC Pvt. Ltd. The properties of the Nb metal are shown in Table 1. The samples were cut into 15 mm × 15 mm plates using a laser cutting equipment with 2 kW fiber laser. Then the cut samples were further polished using a SiC grinding disk upto #P1200 sizing. Further, the grinded samples were mirror polished using Memphis cloth with the help of 1 μm diamond-based grinding paste.

Oxidation test was carried out in a box furnace (Carbolite-Gero,

* Corresponding authors.
E-mail addresses: k1825123@kingston.ac.uk (K. Ramachandran), k1635402@kingston.ac.uk (Y.C. Jayakody), d.daniel@kingston.ac.uk (D.D. Jayaseelan).

https://doi.org/10.1016/j.ijrmhm.2022.106033
Received 16 June 2022; Received in revised form 13 October 2022; Accepted 17 October 2022
Available online 26 October 2022

Table 1
Properties of Nb obtained from the manufacturer.

Properties	Density	Melting point	Thermal conductivity	Youngs modulus	Thermal expansion coefficient
Values	8.50 g/cm^3	2476 °C	54 W/m. K	170 GPa	7.3 μm/m. °C

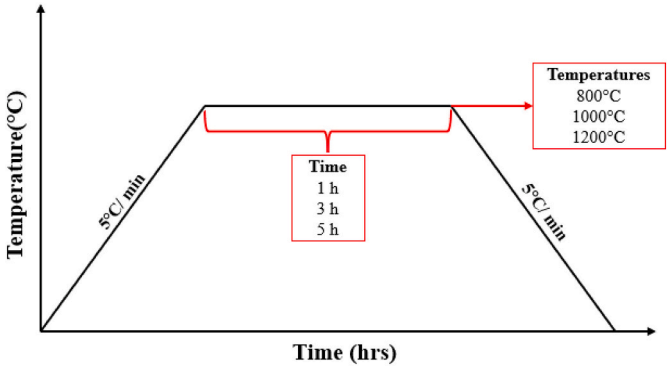

Fig. 1. Temperature profile for oxidation studies on Nb metal.

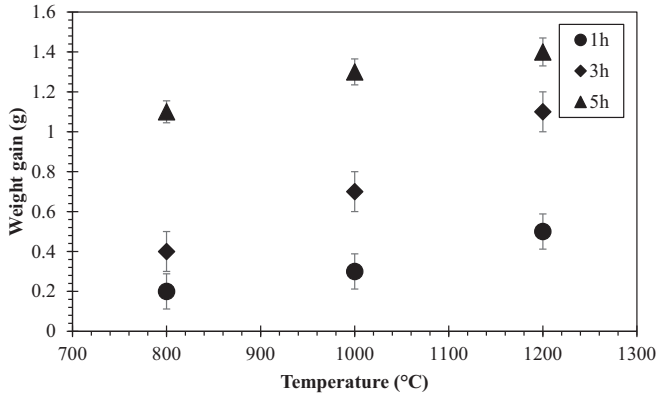

Fig. 2. Weight Gain of Nb metal with respect to time and temperature.

Germany) at 800 °C, 1000 °C and 1200 °C for different time intervals of 1, 3 & 5 h. The samples were placed on the alumina boats such that they had minimum contact between alumina and edges of samples. The samples were heated at a rate of 5 °C/min and cooling rate were kept at 5 °C/min as illustrated in temperature profile in Fig. 1.

The Nb samples before and oxidation studies were characterised using techniques like scanning electron microscopy (Zeiss SM350D) fitted with EDS and X-ray diffraction (XRD) (Burker D8) to identify the phases formed. XRD analysis was conducted in room temperature (25 °C) with of 2θ values ranging from 0° to 70° with Cu—K with a step time of 0.1°sec^{-1}. Vickers hardness studies were carried out using a diamond intender at a load of 10 kgf and a loading time of 20 s. Three trails were utilised to determine the average hardness of the samples. The indentation fracture toughness of the samples was calculated by measuring the cracks propagated from indentation through Evans Charles equation as illustrated in Eq. (1) where H_V represents Vickers hardness, a represents average half-length of diagonal and c is average half-crack length from diagonal [12–14].

$$K_{IC} \approx 0.203\, H_V \times a^{\frac{1}{2}} \times \left\{\frac{c}{a}\right\}^{-\left(\frac{3}{2}\right)} \quad (1)$$

3. Results and discussion

3.1. Oxidation behaviour

The weight gain of samples after oxidation is plotted in Fig. 2. The initial weight of the Nb sample was measured to be 2.35 g. After oxidation at 800 °C, samples recorded an increase in weight by 8.6%, 17.39% and 47.8% for time intervals of 1, 3 and 5 h, respectively. A similar pattern of increase in weight gain was observed at 1000 °C and 1200 °C with gain of 13.04%, 30.43% and 56.52% for 1000 °C and 21.73%, 47.82% and 60.86% for 1200 °C, respectively. From Fig. 2, it is visible that metal oxidised for long time 5 h, shows the highest weight gain due to the formation of oxide layers onto the samples.

The weight gain at all temperatures at different time intervals shown a linear growth throughout the surfaces of the metals. XRD of oxidised samples indicated formation of Nb_2O_5 which was the most common oxide of niobium [15]. Along with this oxide, formation of a meta-stable phase of $Nb_{12}O_{29}$ was also observed in samples oxidised for shorter time. Fig. 3 (a) & (b) illustrates the XRD peaks of Nb metal after oxidation at 3 h and 5 h at all three different temperatures. From Fig. 3, Nb at low

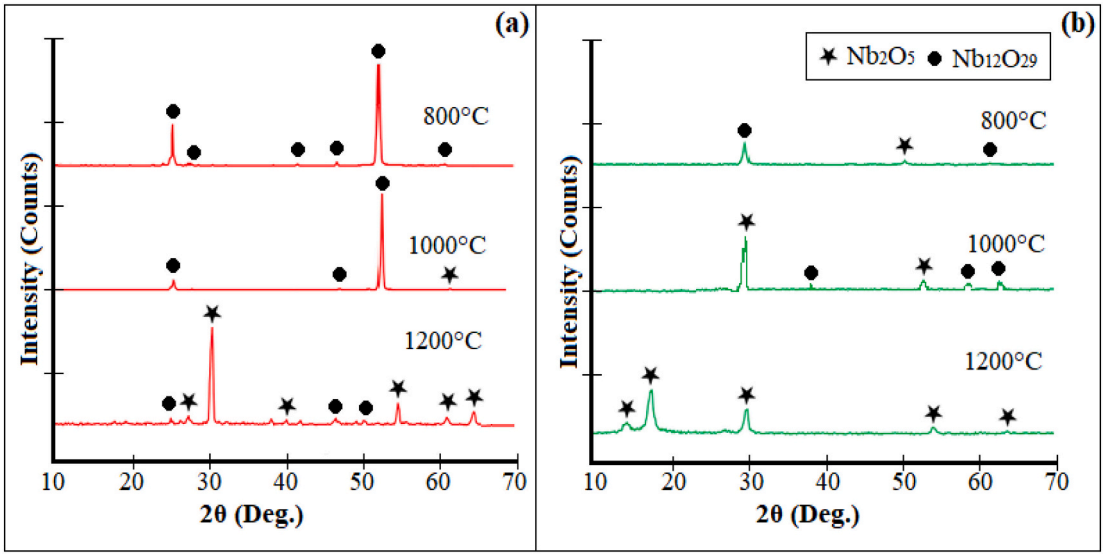

Fig. 3. XRD phases of Nb oxidised at (a) 3 h and (b) 5 h.

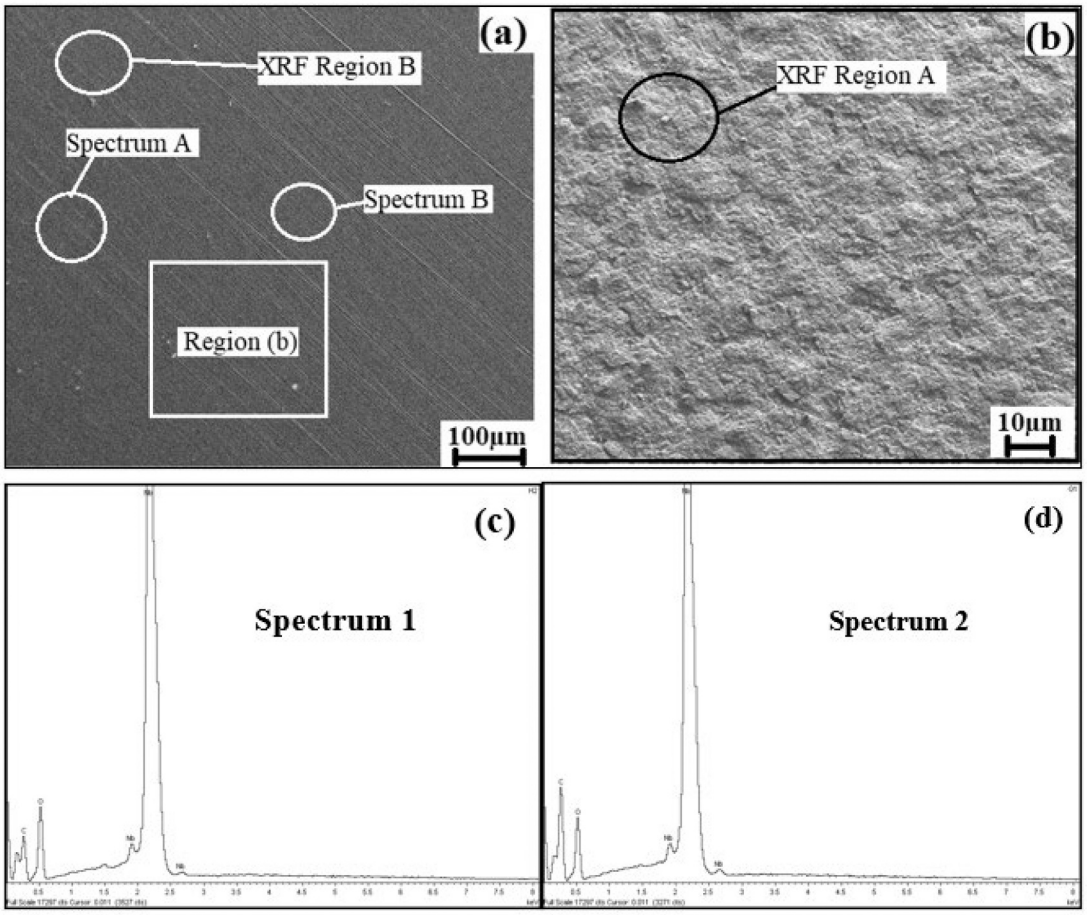

Fig. 4. Scanning electron microscopy and EDS spectrum of pure Nb metal.

Table 2
EDS (Fig. 1(c) &d) and XRF compositions of unoxidized Niobium metal.

Characterisation Technique	Spectrum/ Region	Elemental Composition (Wt%)			
		Niobium (Nb)	Oxygen (O)	Iron (Fe)	Manganese (Mn)
EDS	Spectrum A	99.78	0.22	0.00	0.00
	Spectrum B	99.91	0.09	0.00	0.00
XRF	Region A	99.66	0.14	0.08	0.12
	Region B	99.73	0.16	0.03	0.08

temperature (800 °C) led to the formation of $Nb_{12}O_{29}$ which gradually decreased with increase in temperature and time. On the other hand, with gradual increase in temperature, there was also formation of Nb_2O_5 which was visible at samples oxidised for 5 h indicated most peaks corresponded towards the Nb_2O_5. At temperature of 800 °C, weight gain between 1 h and 3 h was restricted due to the formation of meta-stable phase of $Nb_{12}O_{29}$ which inhibited further oxidation of metal substrate. The formation of the meta-stable phase of Nb led to steep weight gain at 900 °C at 1 h.

Although there have been studies on the formation of Nb_2O_5 on the surfaces of Nb metal as per Eq. (2), the formation of meta-stable oxide passivation layer of the Nb has not been mentioned elsewhere. Eq. (3) shows the formation reaction of meta-stable oxide phase of the Nb and owing to high concentration of oxygen molecules present in the phase, it tends to be unstable and decomposes back to stable oxide of niobium at high temperature by reacting with additional atmospheric oxygen as given in Eq. (4). The formation of the H-Nb_2O_5 at high temperature and atmospheric conditions is said to be highly stable polymorph of niobium oxide which forms at temperature range of 1000 °C [16].

$$4\ Nb\ (s) + 5\ O_2(g) \rightarrow 2\ Nb_2O_5\ (s) \quad (2)$$

$$24\ Nb\ (s) + 29\ O_2(g) \rightarrow 2Nb_{12}O_{29}\ (s) \quad (3)$$

$$2\ Nb_{12}O_{29}\ (s) + O_2(g) \rightarrow 12\ Nb_2O_5(s) \quad (4)$$

The SE image in Fig. 4 shows the surface of pure Nb metal at two different magnifications. The corresponding EDS and XRF results provided in Table 2 confirms the high purity of the metal. The EDS and XRD results show that there is a trace of pre-oxidation at room temperature. Although, EDS did not showcase any traces of Fe or Mn, XRF indicated small traces which could have been the impurities.

Fig. 5(a) indicates the surface of Nb metal after oxidation for 3 h at 800 °C. Comparing the non-oxidised surface in Fig. 4(a), surface shows dark spots throughout the region and with increase in the oxidation temperature, the metal initiates to lose its surface smoothness leading to formation of uneven surfaces throughout the material (Fig. 5(b-d)). This could have been due to the formation of passive oxidation layers. Fig. 5 (b) indicates that Nb oxidised at 800 °C for 5 h shows the presence of surface rip off through SE imaging. With increase in temperature to 1000 °C, surface rips enhance leading to formation of small nodes throughout the surface. The features on the surfaces of metal could be due to the formation of Nb_2O_5 which is said to have a palish grey colour. Further, continuous passivation layers of metastable $Nb_{12}O_{29}$ which was visible in Fig. 5(b) starts to decompose leading to cracks. XRD results indicates the formation of Nb_2O_5 which could be confirmed by its corresponding SE image in Fig. 5(c & d) with a formation of granules. This is also supported via EDS and XRF analysis tabulated in Table 3. EDS and

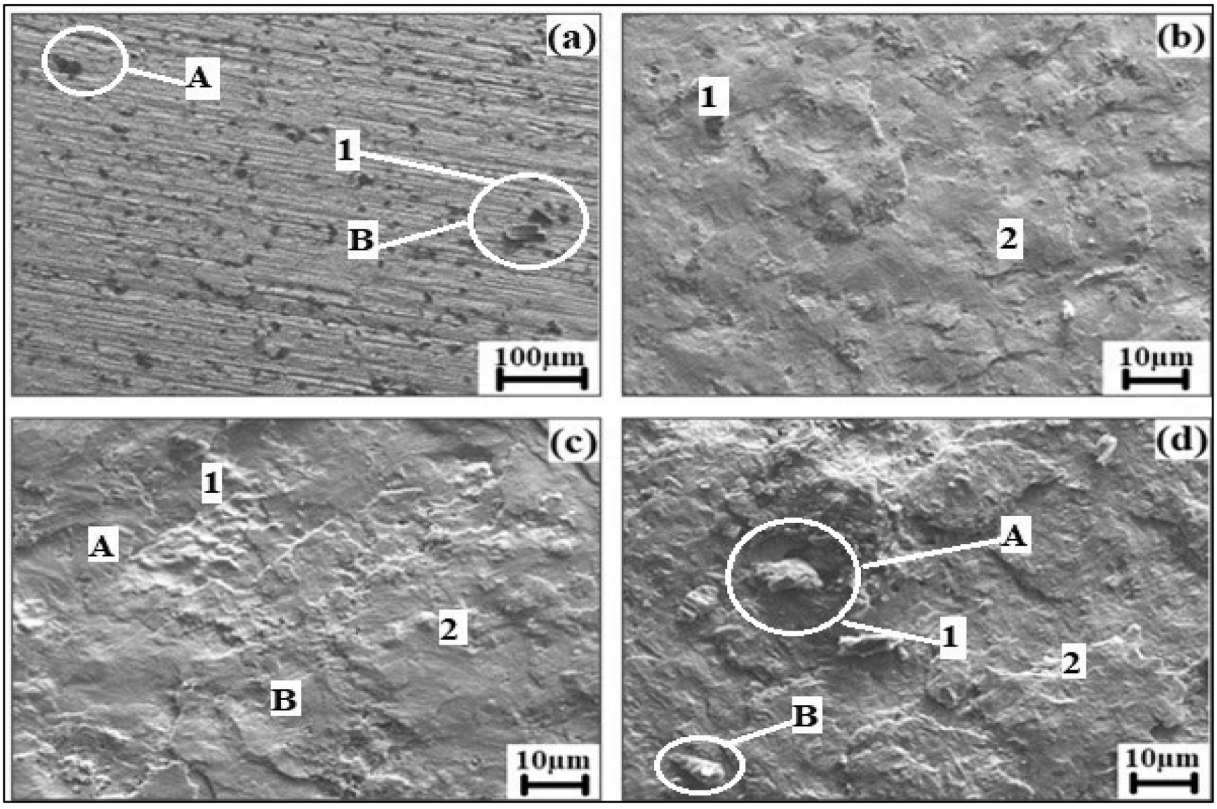

Fig. 5. Scanning electron images of (a) metal oxidised at 800 °C for 3 h (b) metal oxidised at 800 °C for 5 h (c) oxidisation at 1000 °C for 3 h and (d) oxidation at 1000 °C for 5 h.

Table 3
Elemental composition of Fig. 5 characterised via EDS and XRF techniques.

Nomenclature	Characterisation Technique	Region/Spectrum	Elemental Composition (Wt%)			
			Nb	O	Fe	Mn
Fig. 5(a)	EDS	Spectrum A	71.60	28.40	–	–
		Spectrum B	71.26	28.74	–	–
	XRF	Region 1	68.26	31.52	0.13	0.09
		Region 2	70.49	29.48	–	0.03
Fig. 5(b)	XRF	Region 1	57.16	42.83	–	0.01
		Region 2	56.26	43.71	–	0.04
Fig. 5(c)	EDS	Spectrum A	28.58	71.42	–	–
		Spectrum B	28.65	71.35	–	–
	XRF	Region 1	32.68	67.19	0.09	0.04
		Region 2	38.78	61.22	–	–
Fig. 5(d)	EDS	Spectrum A	27.9	72.1	–	–
		Spectrum B	28.3	71.7	–	–
	XRF	Region 1	27.86	72.11	0.01	0.02
		Region 2	27.35	72.65	–	–

XRF tabulated in Table. 3 indicates presence of oxygen element on the surfaces of Nb metal in different elemental percentages. In Fig. 5(c), spectrums of EDS and XRF indicated higher elemental content of oxygen to niobium indicating formation of metastable phase of $Nb_{12}O_{29}$ which was also confirmed via XRD analysis. Further, analysis indicated that the composition drops to a percentage equal to Nb_2O_5 supporting the diffusion of metastable phase to highly stable Nb penta-oxide phase.

SE image of Nb substrate oxidised at 1200 °C at 5 h is shown in Fig. 6. From Fig. 6, it could be observed that surface had dark phases with cracks propagating from the phase the brittle behaviour of the oxide ceramics forming on the surfaces [13,14]. Further, no passivation layer could be detected on the surfaces justifying the XRD which indicated complete conversion of $Nb_{12}O_{29}$ to Nb_2O_5. A closer observation of dark spot is provided in Fig. 6(b) which shows presence of micro-pores throughout the dark spots with cracks. The continuous formation of oxide layers on the surface could lead to prominent drop in the mechanical properties. EDS analysis on the surfaces illustrated in Table. 4 indicates only traces of Nb and O throughout all the spectrums. The EDS supported the full formation Nb_2O_5 throughout all the spectrums with oxygen having higher elemental composition compared to niobium.

Pilling Bedworth ratio was utilised for to investigate the presence of formation of meta-stable phases since it accounts to the ratio between the molar volumes of metal oxide and metal and was calculated 2.66 and 1.319 for Nb_2O_5 and $Nb_{12}O_{29}$ respectively using Eq. (5) BP ratio [17].

$$R = \frac{(W/\mathrm{D}) \times (f)}{w/d} \tag{5}$$

where R is Pilling Bedworth ratio, W is molecular weight of oxide per

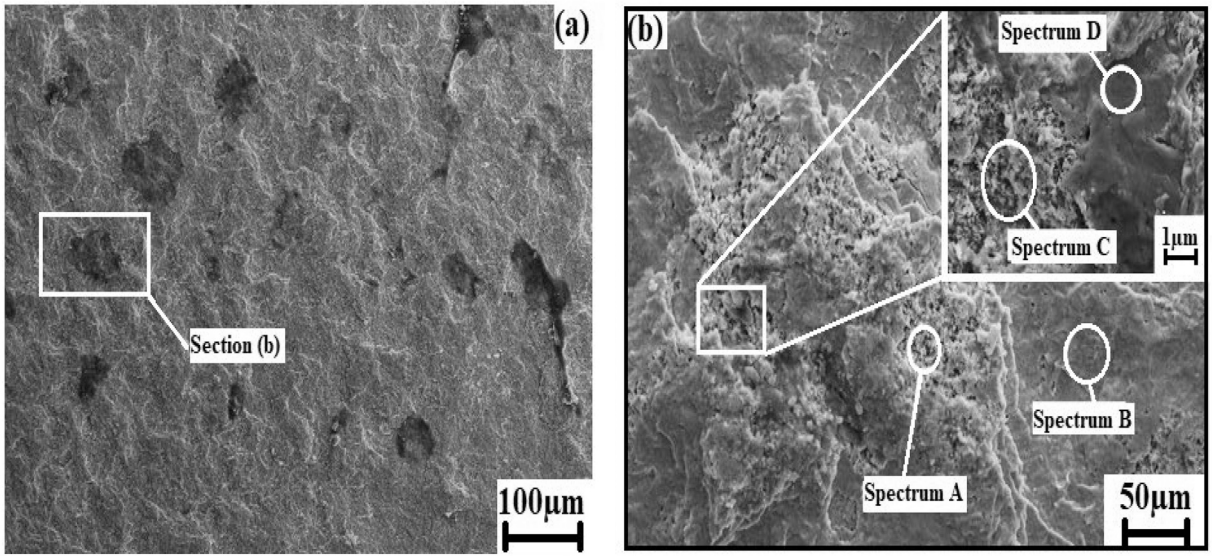

Fig. 6. SE image of Nb metal after oxidation at 1200 °C for 5 h.

Table 4
Vickers hardness & fracture toughness of Nb before and after oxidation.

Oxidation State	Condition	Vickers Hardness (GPa)	Fracture Toughness (MPa. $m^{1/2}$)
Pre-Oxidation	RT	5 ± 0.5	40.6 ± 0.5
Oxidised Samples	800 °C/5 h	5.6 ± 0.3	33.2 ± 0.8
	1000 °C/5 h	6.4 ± 0.2	30.6 ± 0.3
	1200 °C/5 h	8.06 ± 0.4	28.14 ± 0.4

mol, D is specific density of oxide, f is factor per mol of oxidant, w is themolecular weight of oxidising metal per mol, and d is specific density of metal. As per Pilling Bedworth ratio of $Nb_{12}O_{29}$ which satisfies "$0<Nb_{12}O_{29}< 2$", it allows the formation of a passivation layer without cracks or chipping while covering the entire surface. For this case samples oxidised for 1000 °C confirmed via SE results in Fig. 5(d) which shows a full passivation layer formed covering the once exposed substrate. However, when converted to Nb_2O_5 does not permit the formation of a passivation layer as it satisfies "$Nb_2O_5 >2$" which dictated that the formation of metal oxide is of an excess which creates cracks and chippings, this is evident in samples oxidised at 1200 °C for 5 h as shown in Fig. 6. This is due to the brittle nature of Nb_2O_5 and inability of plastic deformation which promotes to cracking hence oxidising the substrate. The brittle behaviour of the oxide formation onto Nb metal were supported through the Vickers hardness and its following indentation fracture toughness of Nb metal pre and after oxidation is tabulated in Table 4 by measuring the cracks propagated by indentation through a microscope. The metal showed a hardness of 5 ± 0.5 GPa with an increase to up to 60% for samples oxidised at 1200 °C at the same temperature which is in case for most of the ceramics [7]. Table 4 confirmed that oxidised samples exhibited lower fracture toughness with increased hardness leading to conclusive evidence of the formation of oxide layers which is further confirmed in the oxidation. Sample exposed to 5 h at 1200 °C which was proved to have higher Nb_2O_5 content which corresponded to the lower fracture toughness of 28.14 ± 0.4 MPa. $m^{1/2}$ in comparison with the sample oxidised at 800 °C for 5 h with a lower Nb_2O_5 but higher $Nb_{12}O_{29}$ content corresponding to a better fracture toughness of 33.2 ± 0.8 MPa. $m^{1/2}$.

To further understand the oxidation behaviour of Nb, Gibbs free energies were calculated by determining the enthalpy and entropy changes for the formation of Nb_2O_5. Its Enthalpy was calculated to be

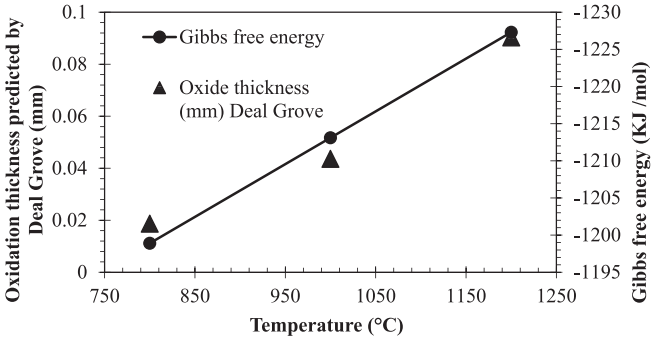

Fig. 7. Gibbs free energy for the formation of Nb_2O_5 and the oxide thickness calculated via the Deal Grove model.

-1161.5 KJ. Mol^{-1} via Eq. (6).

$$\Delta H = \sum Broken\ Bonds - \sum Formed\ Bonds \quad (6)$$

where ΔH is the enthalpy change, sum of broken bonds consists of 5 Oxygen, Oxygen double bonds corresponding to 494 KJ.Mol^{-1} while sum of formed bonds consists of 8 Niobium, Oxygen double bonds corresponding to 513 KJ.Mol^{-1} and 4 Niobium, Oxygen single bonds at 753 KJ.Mol^{-1} in accordance to VESPR diagrams and energy sheets [18]. Calculated Entropy change (-1161.5 KJ.Mol^{-1}) suggests the high stability of the final oxidation stage as Nb_2O_5. Calculated Gibbs free energy values are -1198.90 KJ, -1213.10 KJ and 1227.3 KJ for samples oxidised at 800 °C, 1000 °C and 1200 °C, respectively. This suggests that although the formation of both Nb_2O_5 and $Nb_{12}O_{29}$ are spontaneous reactions, formation of the meta-stable $Nb_{12}O_{29}$ forms first which is followed by its stabilisation. Similarly, the formation of Nb_2O_5 is classified as a spontaneous reaction by its negativity of Gibbs free energy, as it is dependant process. This is supported by T. McQueen et al. who reported formation of unstable structures of $Nb_{12}O_{29}$ out of commercially available Nb_2O_5 most likely due to the inevitable formation of $Nb_{12}O_{29}$ prior to formation of Nb_2O_5 [19]. The linear pattern of the Gibbs free energies as depicted Fig. 7 corresponded with a previous data [20].

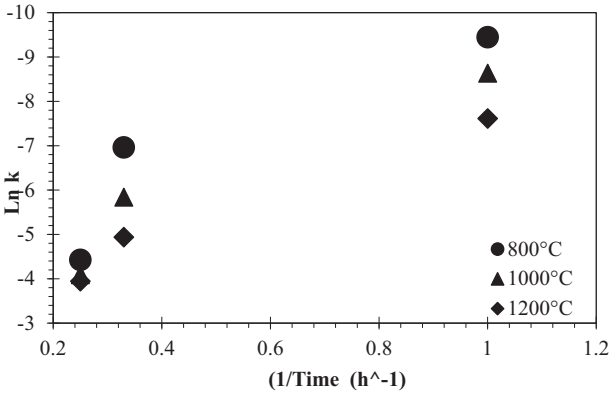

Fig. 8. Arrhenius plots for the formation of Nb_2O_5.

Table 5
Calculated oxidation thickness of Nb metal at different temperatures.

Temperature at which sample oxidises	Oxidation Thickness (mm)
800 °C	0.0187
1000 °C	0.0436
1200 °C	0.0903

3.2. Oxidation thickness prediction

Oxidation is a basic phenomenon which occurs due to molecular diffusion of oxygen with high temperature deformation and swelling due to formation of new products in high temperature alloys and metals [3,21]. While predicting the oxidation thickness, the first consideration which was undertaken was law of Lavoisier which indicates that the mass could neither be created nor destroyed with assumption that there is no flow divergence. Further consideration on the diffusion of any product would not return to its original state. The formed equation to understand the oxide layer thickness was modified for current scenario and Deal Grove equation model is illustrated in Eq. (7) [22].

$$x_0 = \frac{A}{2}\left(\sqrt{1+\frac{4B}{A^2}(t+\tau)}-1\right) \tag{7}$$

where, x_0 is the thickness of the oxidation layer, t is oxidation time, τ accounts for initial oxidation thickness which was taken to be zero due to absence of surface oxidation at initial conditions. Values A and B correspond to constituents of linear and parabolic rate constants for which A was modified to Eq. (8). This was done on the temperatures at focus via the aid of the Arrhenius Equation.

$$A = 2 \times D\left(\frac{1}{k_s}+\frac{1}{h}\right) \tag{8}$$

The rate constant A was obtained via Eq. 6 correspond to $A_{1200^\circ C} = 1.215 \times 10^{-7}$, $A_{1000^\circ C} = 3.605 \times 10^{-8}$, $A_{800^\circ C} = 2.425 \times 10^{-10}$. Where D

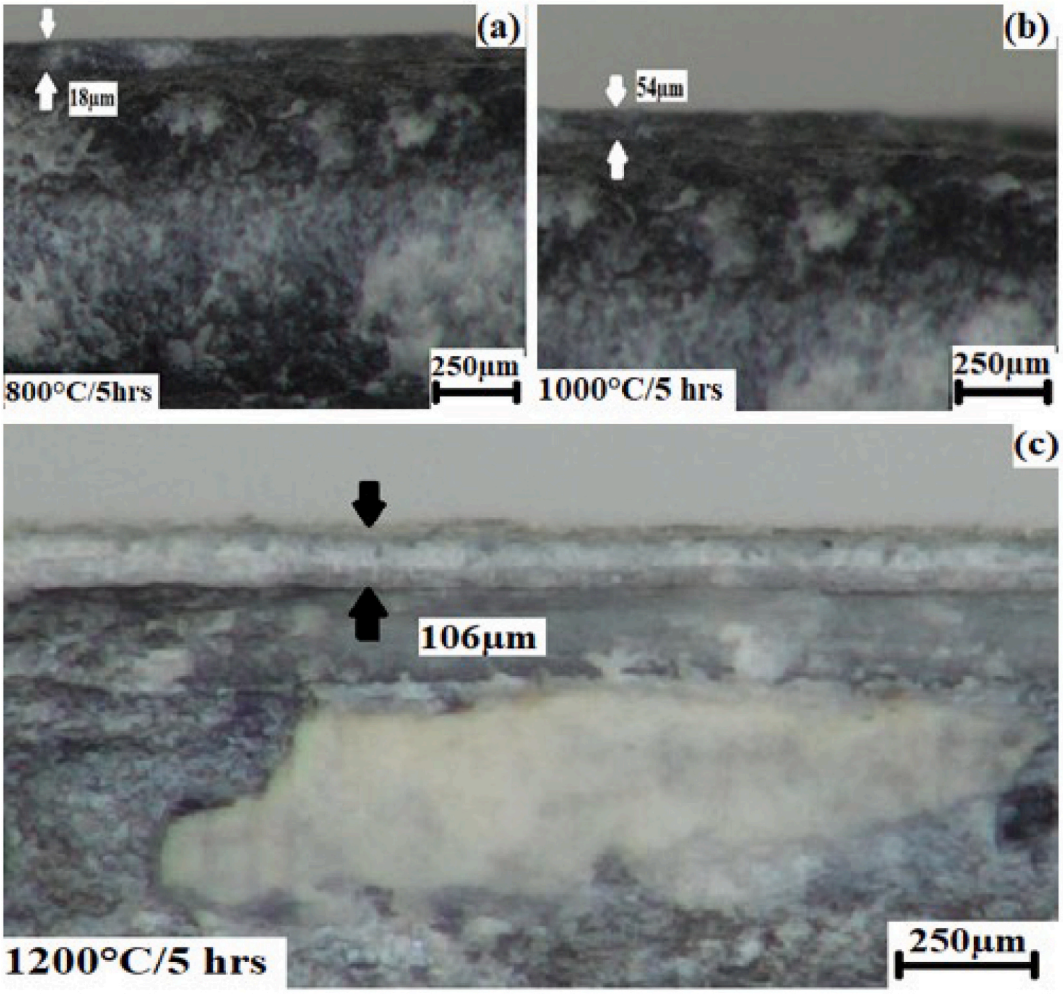

Fig. 9. Oxidation thickness of cross section of Nb observed after (a) 800 °C, (b) 1000 °C and 1200 °C after 5 h.

is the O_2 diffusivity in Nb_2O_5 corresponding to $D_{1200^\circ C} = 1.85 \times 10^{-9}$, $D_{1000^\circ C} = 4.3 \times 10^{-10}$ and $D_{800^\circ C} = 1.72 \times 10^{-12}$ [23]. Gas transportation coefficient of atmospheric air at 1 atm at the respective oxidation temperatures were determined to be $h_{1200^\circ C} = 0.0953\ Wm^{-1}K^{-1}$, $h_{1000^\circ C} = 0.08108\ Wm^{-1}K^{-1}$, $h_{800^\circ C} = 0.07135\ Wm^{-1}K^{-1}$ [24,25]. The Arrhenius constants for the three temperatures 800 °C, 1000 °C and 1200 °C were obtained via extrapolating to the Y-intercept, hence representing the logarithmic value of the Arrhenius constants (Å) as represented in Fig. 8. A represents the frequency at which atoms and molecules collide in a way that leads to a reaction and since the reactions are only present at the surface. Therefore, it was assumed that the Arrhenius constants (A) is equal to surface rate constant K_s in this study. Hence $Å_{1200^\circ C} = K_s = 0.0447$, $Å_{1000^\circ C} = K_s = 0.0338$, $Å_{800^\circ C} = K_s = 0.0177$.

The calculated thickness of the oxidised samples through modified Deal-Grove is reported in Table. 5. From Table 5, it could be seen that thickness was directly proportional to the oxidation temperature. The abrupt increase in the oxidation thickness between 800 °C to 1000 °C was due to degradation of the meta-stable passive oxidation layer of $Nb_{12}O_{29}$ to Nb_2O_5 with increase in the temperature. The cross-sectional view (Fig. 9) of the Nb metal oxidised at 1200 °C for 5 h indicated an oxidation layer thickness of 104 μm which was closer to the calculated value with an error percentage of ~15% which could have due to the inaccuracies while inhibiting the physical properties of the oxide layer owing to chemical constituent which may vary from the characterisation techniques. Further, theoretical Gibbs energy in the phase transformation of the $Nb_{12}O_{29}$ to Nb_2O_5 could be different from the experimental owing to high temperature.

4. Conclusion

The oxidation behaviour of Niobium metal has been studied in atmospheric conditions at high temperatures. The oxidation behaviour of Nb indicated formation of metastable $Nb_{12}O_{29}$ which acted as a protective oxidation layer inhibiting further oxidation beneath Nb metal surfaces at around 800 °C. With increase in temperature, $Nb_{12}O_{29}$ transformed into more stable oxide of Niobium Nb_2O_5. The formation of Nb_2O_5 on the surfaces of Nb metal was said to be unprotective as it exposed the metal substrate for further oxidation resulting in complete formation of oxide. The rate of weight gain for 5 h samples were comparatively lower than 1 and 3 h due to the energy required for phase conversation of $Nb_{12}O_{29}$ to Nb_2O_5 which led to passivation layers to fail. Vickers hardness and its indentation fracture toughness supported the formation of oxide layer as with increase in temperature the fracture toughness of metal decreased by 30%. A mathematical model devised through Deal-Grove equation with relation with Arrhenius equation evidenced the formation of oxide layer thickness which was closer to 10% while measure through electron microscopy.

Declaration of Competing Interest

The authors declare that they have no known competing financial interests or personal relationships that could have appeared to influence the work reported in this paper.

Data availability

Data will be made available on request.

Acknowledgement

Authors Karthikeyan Ramachandran and Yasith C Jayakody would like to acknowledge the support provided by Kingston University, London towards his PhD research. Authors would also like to thank Nery Stival for his contribution towards this research. Authors would also like to thank Mr. Richard Giddens and Mr. Dean Wells, Senior Technicians of Kingston University for their support.

References

[1] J. Sena, M. Merrigan, Survivability tests of foil and screen wicked Niobium-1 percent zirconium/potassium heat pipes, in: 31st Aerospace Sciences Meeting, Reno, NV, USA, 1993.
[2] Y.L. Ge, Y.M. Wang, Y.E. Zhang, L.X. Gou, D.C. Jia, J.H. Ouyang, Y. Zhou, The improved thermal radiation property of SiC doped microarc oxidation ceramic coating formed on niobium metal for metal thermal protective system, Surf. Coat. Technol. 309 (2017) 880–886.
[3] K. Ramachandran, C. Zuccarini, K. Yoshida, T. Tsunoura, D. Jayaseelan, Experimental investigation and mathematical modelling of water vapour corrosion of Ti3SiC2 and Ti2AlC ceramics and their mechanical behaviour, J. Eur. Ceram. Soc. 41 (9) (2021) 4761–4773.
[4] A. Deardo, Niobium in modern steels, Int. Mater. Rev. 48 (6) (2003) 371–402.
[5] W. Wu, Z. Chen, L. Wang, Oxidation behaviour of multilayer iradium coating on niobium substrate, Protect. Metals Phys. Chem. Surf. 51 (4) (2015) 607–612.
[6] X. Guo, Z. Xiao, W. Qiu, Z. Li, Z. Zhao, X. Wang, Y. Jiang, Microstructure and properties of cu-Cr-Nb alloy with high strength, high electrical conductivity and good softening resistance performance at elevated temperature, Mater. Sci. Eng. A 749 (2019) 281–290.
[7] K. Ramachandran, V. Boopalan, J.C. Bear, R.R. Subramani, Multi-walled carbon nanotubes (MWCNTs)-reinforced ceramic nanocomposites for aerospace applications: a review, J. Mater. Sci. 57 (2) (2022) 3923–3953.
[8] D.W. Bridges, W.M.F. Jr, High pressure oxidation of niobium, J. Electrochem. Soc. 103 (6) (1956) 326.
[9] R.H. Truffias, G. Melden, J. Harding, High temperature pxidatio-resistant thurster materials, Phase 2, in: NASA Contractor Report 187205, Cleveland, OH, 1991.
[10] R.A. Perkins, G.H. Meier, The oxidation behavior and protection of niobium, JOM 42 (1990) 17–21.
[11] R. Perkins, K. Chiang, G. Meier, Formation of alumina on Nb-Al alloys, Scr. Metall. 22 (3) (1988) 419–424.
[12] K. Ramachandran, R.R. Subramani, T. Arunkumar, V. Boopalan, Mechanical and thermal properties of spark plasma sintered alumina-MWCNTs nanocomposites prepared via improvised colloidal route, Mater. Chem. Phys. 272 (125034) (2021) 1–9.
[13] T. Arunkumar, K. Ramachandran, R.R. Subramani, M. Anish, T. Jayaraman, R. Boddula, M. Jagannathan, Effect of MWCNTs on improvement of fracture toughness of spark plasma sintered SiC nano-composites, Curr. Anal. Chem. 17 (6) (2021) 849–856.
[14] T. Arunkumar, G. Anand, R. Subbiah, K. Ramachandran, J. Jeevahan, Effect of multiwalled carbon nanotubes on improvement of fracture toughness of spark-plasma-sintered yttria-stabilized zirconia nanocomposites, J. Mater. Eng. Perform. 30 (2021) 3925–3933.
[15] E. Ko, J. Weissman, Structures of niobium pentoxide and their implications on chemical behavior, Catal. Today 8 (1) (1990) 27–36.
[16] J.L. Waring, R.S. Roth, H.S. Parker, Temperature-pressure phase relationships in niobium pentoxide, J. Res. Nat. Inst. Stand. Technol. 77A (6) (1973) 705–711.
[17] C. Xu, W. Gao, Pilling-Bedworth ratio for oxidation of alloys, Mater. Res. Innov. (2016) 231–235.
[18] Y.-R. Luo, Bond Dissociation Energies, in: Handbook of Bond Dissociation Energies in Organic Compounds, CRC Press, Boca Raton, 2022, pp. 66–98.
[19] T. McQueen, Q. Xu, E. Andersen, H. Zandbergen, R. Cava, Structures of the reduced niobium oxides Nb12O29 and Nb22O54, J. Solid State Chem. (2007) 2864–2870.
[20] S. Venkataraj, R. Drese, C. Liesch, O. Kappertz, R. Jayavel, M. Wuttig, Temperature stability of sputtered niobium–oxide films, J. Appl. Phys. 91 (8) (2002) 4863.
[21] K. Loeffel, L. Anand, Z.M. Gasem, On modeling the oxidation of high-temperature alloys, Acta Mater. 61 (2) (2013) 399–424.
[22] S.K. Gupta, A. Azam, R. Bhatia, R. Soni, J. Akhtar, Determination of face terminated wet thermal oxidation rates in 4H-SiC Substrate, in: National Conference on Electronic Technology (ECT-2010), Goa, India, 2010.
[23] W.K. Chen, R.A. Jackson, Diffusion of oxygen in near-stoichiometric α-Nb2O5, J. Chem. Phys. 47 (1144) (1967).
[24] A.B. Murphy, Transport coefficients of air, argon-air, nitrogen-air, and oxygen-air plasmas, Plasma Chem. Plasma Process. 15 (1995) 279–307.
[25] V.Ya. Rudyak, E.V. Lezhnev, Stochastic algorithm for simulating gas transport coefficients, J. Comput. Phys. 355 (2018) 95–103.